Original article

Nuclear Medicine Communications

Quantitative analyses of [^{11}C]Ro15-4513 binding to subunits of GABA$_A$/benzodiazepine receptor in the living human brain

Yoshiyuki Asai[a,b], Yoko Ikoma[a], Akihiro Takano[a], Jun Maeda[a], Hinako Toyama[c], Fumihiko Yasuno[a], Tetsuya Ichimiya[a], Hiroshi Ito[a] and Tetsuya Suhara[a]

Background **Gamma-aminobutyric acid (GABA)$_A$/benzodiazepine (BZ) receptor chloride channel consists of several subunits. The diversity of the α subunits results in the various ligand selectivity and functionally different properties of the GABA$_A$/BZ receptor. Although [^{11}C]Ro15-4513 is reported to be a radioligand that has relatively high affinity for α5 subunit-containing GABA$_A$/BZ receptor, it remained to be evaluated fully.**

Aim **The aim of this study was to evaluate the quantitative analyses of [^{11}C]Ro15-4513 in the living human brain.**

Methods **Positron emission tomography examinations were performed in eight healthy male volunteers after intravenous injection of [^{11}C]Ro15-4513. Kinetic analysis of data was performed with the two-compartment and three-compartment models using arterial input function. Linear graphical analysis and the simplified reference tissue model analysis (SRTM) were also performed using pons as a reference region. In a simulation study, the effects of noise to the estimation of binding potentials were evaluated.**

Results **The accumulation of [^{11}C]Ro15-4513 in the limbic system was relatively higher than in other cortex. The bindings were well described by the three-compartment model in the regions with specific binding. Binding potentials obtained from the graphical method and SRTM correlated well with those obtained from the three-compartment model. In the simulation study, estimated parameters from SRTM were less affected by noise compared with those from the graphical method.**

Conclusion **The reference tissue methods using pons as a reference region can be used for quantitative analysis of [^{11}C]Ro15-4513 binding. SRTM seemed less susceptible to noise than does graphical analysis. *Nucl Med Commun* 30:872–880 © 2009 Wolters Kluwer Health | Lippincott Williams & Wilkins.**

Nuclear Medicine Communications 2009, **30**:872–880

Keywords: benzodiazepine, [^{11}C]Ro15-4513, compartment analysis, positron emission tomography

[a]Molecular Neuroimaging Group, Molecular Imaging Center, National Institute of Radiological Sciences, Chiba, [b]Department of Psychiatry, Division of Neurological Science, Hokkaido University Graduate School of Medicine, Sapporo and [c]Department of Health Service Management, International University of Health and Welfare, Ohtawara, Japan

Correspondence to Tetsuya Suhara, MD, PhD, Molecular Neuroimaging Group, Molecular Imaging Center, National Institute of Radiological Sciences, 4-9-1 Anagawa, Inage-ku, Chiba, 263-8555, Japan
Tel: +81 43 206 3251; fax: +81 43 253 0396; e-mail: suhara@nirs.go.jp

Received 27 October 2006 **Revised** 30 December 2006
Accepted 2 June 2007

Introduction

The central benzodiazepine (BZ) binding sites are located in the γ-aminobutyric acid (GABA$_A$)/BZ receptor chloride channel complex [1]. Central BZ receptors have been implicated in several neuropsychiatric diseases [1,2]. Central BZ receptors have been visualized using positron emission tomography (PET) with several ligands such as [^{11}C]flumazenil and [^{11}C]Ro15-4513 [3–10]. Both [^{11}C]flumazenil and [^{11}C]Ro15-4513 have the imidazobenzodiazepine core structure (Fig. 1). However, flumazenil is a BZ receptor antagonist, whereas Ro15-4513 is known as a BZ receptor partial inverse agonist. A different distribution pattern has been reported for the binding of [^{11}C]Ro15-4513 compared with that of [^{11}C]flumazenil [6–8,11]. Different affinity to subunits that compose GABA$_A$/BZ receptor chloride channel complex has been suggested to explain the difference [11,12]. GABA$_A$/BZ receptor chloride channel complexes are revealed to consist of two α subunits, two β subunits, and one γ subunit [2,13,14]. Ro15-4513 has relatively higher affinity for the α5 subunit-containing GABA$_A$/BZ receptor than the other types of α subunits *in vitro* [15,16], whereas flumazenil binds nonselectively to the GABA$_A$/BZ receptor [4,5,7]. Our previous study, in monkeys, indicated that the high accumulation of [^{11}C]Ro15-4513 in the frontotemporal limbic regions would represent the binding to the GABA$_A$/BZ receptor α5 subunit [17].

It has been reported that the diversity of the α subunits results in the various ligand selectivity and functional properties of the GABA$_A$/BZ receptor [2,14,18–25]. α1 subunits have been suggested to be related to hypnotic and sedative amnesic actions, whereas the α2, α3, and α5

0143-3636 © 2009 Wolters Kluwer Health | Lippincott Williams & Wilkins DOI: 10.1097/MNM.0b013e32833019bf

Fig. 1

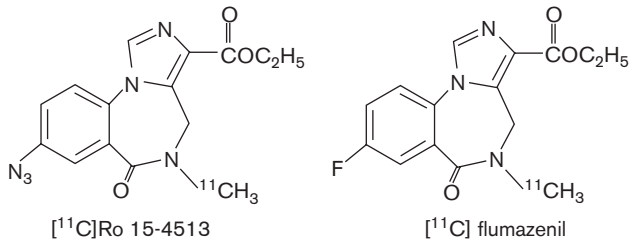

Chemical structure of [^{11}C]Ro15-4513 and [^{11}C] flumazenil.

subunits are related to anxiolytic, anticonvulsant, and antipsychotic actions [26,27]. Furthermore, several studies were reported to investigate the relationship between α subunits and psychiatric or neural diseases [28–35].

Although [^{11}C]Ro15-4513 was developed in the early 1990s [6,7], its use as a PET ligand has been limited because of the uncertainty about which $GABA_A$/BZ receptor was being labeled. With the recent investigation of subunits of the $GABA_A$/BZ receptor, [^{11}C]Ro15-4513 has begun to be reevaluated [17,36]. Although distribution volumes of [^{11}C]Ro15-4513 were measured using spectral analysis in a recent study [36], the quantitative method of [^{11}C]Ro15-4513 has not been fully evaluated. In addition, as further clinical application of this radioligand was expected, simplified quantitative analysis would also be required. In this study, we aimed to perform the quantitative analysis of [^{11}C]Ro15-4513 in the living human brain. The standard two-compartment and three-compartment models with a metabolite-corrected plasma input function were evaluated. Simplified methods without arterial blood sampling were also evaluated for further clinical study.

Materials and methods

Participants

Eight healthy male volunteers (mean age 23.8 ± 4.0 years, range 21–31 years) participated after giving informed consent. Participants were screened for history of psychiatric illnesses, chronic somatic illnesses, and substance abuse. None of them was taking any drugs. This study was approved by the Ethics and Radiation Safety Committee of the National Institute of Radiological Sciences, Chiba, Japan.

Radiochemistry

[^{11}C]Ro15-4513 was synthesized by *N*-methylation of a corresponding *N*-desmethyl precursor with [^{11}C]methyl iodide. The reaction mixtures were purified by liquid chromatography (LC) and eluted with CH_3CN/6 mmol/l phosphoric acid = 175/325. The radiochemical purities were more than 95%.

Positron emission tomography system and experimental procedures

The PET system was ECAT EXACT HR + (CTI-Siemens, Knoxville, Tennessee, USA), which provides 63 planes and a 15.5-cm field of view and used in three-dimensional mode. In each scan, a cannula was inserted into the left radial artery for blood sampling and another cannula into the right antecubital vein for radioligand injection. After a transmission scan with a ^{68}Ge–^{68}Ga source, a bolus of 196.47–415.51 MBq (316.35 ± 95.56 MBq, mean ± SD) of [^{11}C]Ro15-4513 was injected intravenously with a 20 ml saline flush. The specific radioactivity was 13.87–174.96 GBq/μmol (97.28 ± 48.04 GBq/μmol, mean ± SD) at the time of injection. Radioactivity in the brain was measured in a series of sequential frames (from 20 s to 10 min for each frame) for up to 60 min (total 28 frames). All emission scans were reconstructed with a Hanning filter cut-off frequency of 0.4 cycle/pixel (full-width at half-maximum 7.5 mm).

Arterial blood sampling

Arterial blood samples were taken manually at 20, 30, 40, 50, 60, 70, 80, 90, 100, 110, 130, 150 s, 3, 5, 7, 10, 15, 20, 30, 45, and 60 min after the radiotracer injection. Samples to determine radioactive metabolites in plasma were drawn at 2, 4, 9, 14, 19, 40, and 59 min after the radiotracer injection. Radioactivity in the plasma fraction was counted using a Cobra II γ-counter (Packard Instrument Company, Downers Grove, Illinois, USA) cross-calibrated with the PET system.

Determination of ligand metabolism in the plasma

In each experiment, the fraction of the plasma radioactivity representing unchanged [^{11}C]Ro15-4513 was determined by high-performance LC (HPLC). Arterial plasma samples (0.7 ml) were deproteinized with acetonitrile and analyzed by HPLC for metabolites. HPLC analysis was performed using a Waters μ-Bondapak C18 column (7.8 × 300 mm, 10 μm) using 50 : 50 CH_3CN + 6 mmol/l phosphoric acid at 2.5 ml/min.

MRI scans

T1-weighted magnetic resonance images (MRI) of the brain were obtained for all participants using a 1.5 T Gyroscan NT (Phillips Medical Systems, Best, Netherlands).

Regions of interest

PET images were coresigtered to MRI using SPM99 (Wellcome Department of Imaging Neuroscience, UK). Seven regions of interest (ROIs) were drawn on the MRI manually and transferred on the coregistered PET images. ROIs were delineated for the pons, hippocampus, amygdala, anterior cingulate cortex, insular cortex, lateral temporal cortex, and occipital cortex.

Fig. 2

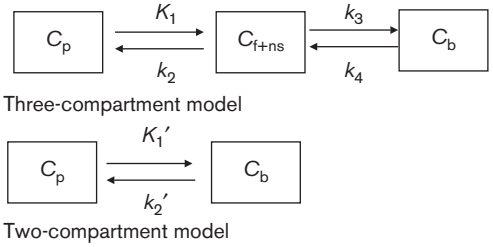

Two-compartment and three-compartment models used for kinetic data analysis of [^{11}C]Ro15-4513 binding.

Kinetic analysis

Kinetic data analysis was performed based on the two-compartment and three-compartment models (Fig. 2). The three-compartment model includes: the radioactivity concentration of unchanged radioligand in plasma (C_p), the concentration of free and nonspecifically bound radioligand (C_{f+ns}), and the concentration of specifically bound radioligand (C_b). The rate constants K_1 and k_2 correspond to the influx and efflux rates from plasma to the tissue compartments. The rate constants k_3 and k_4 describe the binding and dissociation at the specific binding compartment. On the basis of this model, the time–activity curve is expressed as the following differential equations:

$$dC_{f+ns}(t)/dt = K_1 C_p(t) - (k_2 + k_3) C_{f+ns}(t) + k_4 C_b(t) \quad (1)$$

$$dC_b(t)/dt = k_3 C_{f+ns}(t) - k_4 C_b(t) \quad (2)$$

$$C_t(t) = C_{f+ns}(t) + C_b(t) \quad (3)$$

where $C_t(t)$ is the radioactivity concentration in brain, as measured by PET. The ratio k_3/k_4 corresponds to the ratio receptor density (B_{max})/dissociation constant (K_d) and is often referred to as the binding potential (BP) [37]:

$$BP = k_3/k_4 = B_{max}/K_d \quad (4)$$

The two-compartment model includes the radioactivity concentration of unchanged radioligand in plasma (C_p), the concentration of radioligand in the brain (C_t). Assuming that the concentrations C_{f+ns} and C_b equilibrate rapidly, they are combined in one single compartment (C_t).

Nonlinear least square fitting analyses

For the two-compartment and three-compartment models, rate constants were estimated for all ROIs by nonlinear least square fitting (NLSF) using the Levenberg–Marquardt algorithm [38], and goodness of fit was evaluated by *F*-test statistics, Akaike information criterion (AIC) [39] and Schwarz criterion (SC) [40]. For the *F*-test:

$$F = \frac{(RSS_{2CM} - RSS_{3CM})/(N_{3CM} - N_{2CM})}{RSS_{3CM}/(n - N_{3CM})} \quad (5)$$

AIC and SC are defined as follows:

$$AIC = n \log_e(RSS) + 2N \quad (6)$$

$$SC = n \log_e(RSS) + N \log_e n \quad (7)$$

$$RSS = \sum_{i=1}^{n} (R_i' - R_i)^2 \quad (8)$$

where n is the number of frames, N is the number of parameters in the model, RSS is the residual square sum, R_i' is the regional radioactivity of fitting curve, R_i is the regional radioactivity of measured time–activity curve, 2-CM is the two-compartment model and 3-CM is the three-compartment model. *F*-statistics have (2,24) degrees of freedom, and an *F*-value greater than 3.40 indicates statistically better fitting with the three-compartment model than with the two-compartment model ($P < 0.05$). Lower AIC and SC values indicate a better fit. For the three-compartment model, BP was calculated from the ratio k_3/k_4 and is referred as BP_{3CM}.

The pons is a region that is almost devoid of the $GABA_A$/BZ receptor complex [5]. In a region with no specific binding sites, the two-compartment model without specific binding compartment (C_b) would be sufficient to describe the time–activity curves and the fitting was evaluated with two-compartment and three-compartment models.

Simplified method analyses

Simplified methods without arterial blood sampling were applied to determine BP values because the pons would be used as the reference tissue. Several simplified methods were evaluated based on the comparison with BP values obtained from the kinetic modeling approach.

Linear graphical analysis without blood sampling

[^{11}C]Ro15-4513 binding was also analyzed by graphical analysis without blood sampling [41]. This method uses the radioactivity concentration of the reference region without a specific binding site, and distribution volume (DV) ratio (DVR) of target and reference region is estimated as a slope. In this study, the pons was used as the reference region. If K_1/k_2 in the reference and target regions are equal, the BP is given by the equation:

$$BP = DVR - 1 \quad (9)$$

where $DVR = DV_{ROI}/DV_{pons}$ is obtained by graphical analysis without blood sampling. The BP calculated with this analysis is referred as $BP_{graphical}$.

Simplified reference tissue model analysis

Simplified reference tissue model (SRTM) analysis [42] was also performed using the pons as the reference region. In brief, based on the three-compartment model, regional radioactivities in a target region (C_T) can be described by the following equation:

$$C_T(t) = R_1 C_R(t) + (k_2 - R_1\theta_3) C_R(t) * e_3^{-\theta} t \qquad (10)$$

where C_R represents the radioactivity in the reference region, R_1 is the ratio of K_1 in a target region to the reference region, $\theta_3 = k_2/(1 + BP)$, K_1 and k_2 are rate constants corresponding to the influx and efflux rates from plasma to the tissue compartments, and * is the convolution operator. The BP calculated with this analysis is referred as BP_{SRTM}.

Simulation study

The effects of noise on the estimation reliability of graphical analysis without blood sampling and simplified reference tissue model analysis were evaluated by a computer simulation [43]. Simulated time–activity curves for the insular cortex, which showed highest accumulation in the brain, and the pons, which was used as a reference region, were generated with several noise levels. A dynamic tracer concentration was derived from the rate constants and a measured input function according to the human PET imaging protocol. The true rate constants determined from the measured data of one participant were: $K_1 = 0.58$, $k_2 = 0.70$, $k_3 = 0.94$, $k_4 = 0.14$, $BP = 6.7$ for the insular cortex, $K_1 = 0.30$, $k_2 = 0.36$ for the pons. The noise level for each frame was determined according to the collected total count given by the equation (12), and noise with Gauss distribution was added to each time–activity curve.

$$N(t) = f \int_{t-t_d/2}^{t+t_d/2} Ct(t') \exp\left(-\frac{\log_e 2}{T} t'\right) dt' \qquad (11)$$

$$\text{Noise}(\%) = \frac{\sqrt{N(t)}}{N(t)} \times 100 = \frac{1}{\sqrt{N(t)}} \times 100 \qquad (12)$$

where C_t is the nondecaying tissue radioactivity concentration derived from the rate constants and the input function, t_d is the data collection time, T is the physical half-life of the radionuclide, and f is a scaling factor representing the sensitivity of the measurement system and is introduced here to adjust the noise level. Seven datasets with noise levels of 1, 3, 5, 7, 10, 15, and 20% at the last frame were created. BPs were estimated with graphical analysis without blood sampling and SRTM analysis for these simulated time–activity curves, and the relationship between the reliability of estimated parameter and noise level was investigated for both methods. The reliability was evaluated by the mean and coefficient of variance [COV; SD/mean (%)] of estimated BPs for 1000 noise realizations at each noise level.

Results

After an intravenous injection of [^{11}C]Ro15-4513, the radioactivity appeared rapidly in the brain. The accumulations of [^{11}C]Ro15-4513 in the hippocampus, amygdala, anterior cingulate cortex, and insular cortex were relatively higher than those in other cortical regions (Fig. 3). The time–activity curves for regional brain radioactivity in one participant are shown in Fig. 4. Radioactivity peaked between 1 and 4 min in the pons and occipital cortex, between 3 and 12 min in the anterior cingulate cortex, insular cortex, and lateral temporal cortex, and between 5 and 20 min in the hippocampus and amygdala.

The fraction of unchanged [^{11}C]Ro15-4513 in plasma was approximately $40.5 \pm 8.2\%$ at 9 min and $24 \pm 5.7\%$ at 59 min after injection (Fig. 5a). The representative curves for total and unchanged radioligand in plasma of one participant are shown in Fig. 5b. After an intravenous injection of [^{11}C]Ro15-4513, radioactivity in the plasma peaked at about 1 min and decreased rapidly. The plasma

Fig. 3

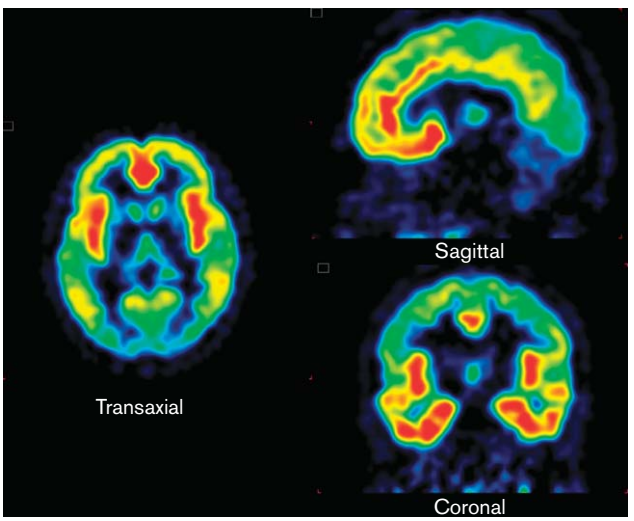

[^{11}C]Ro15-4513 PET images of one participant in three projections, obtained by summation of late-time frames (30–60 min). The participant's right is on left in transaxial and coronal projection. Anterior is on the left in sagittal projection.

Fig. 4

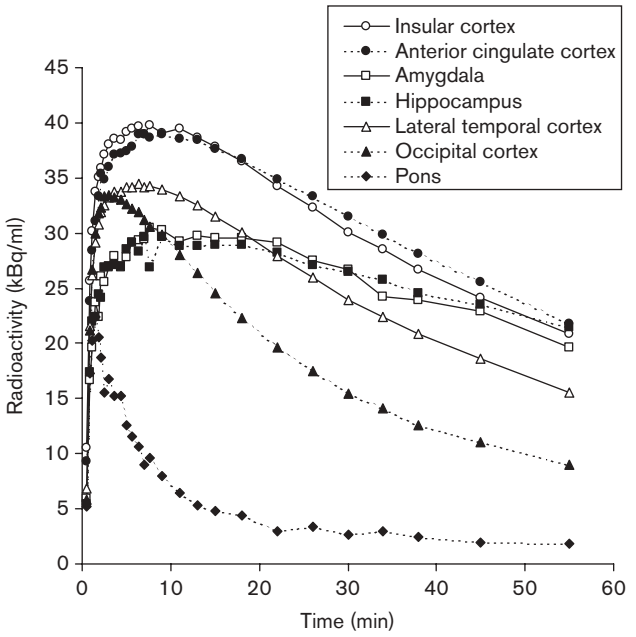

Time–activity curves for regional brain radioactivity after intravenous injection of 378.14 MBq of [^{11}C]Ro15-4513 in one participant.

Fig. 5

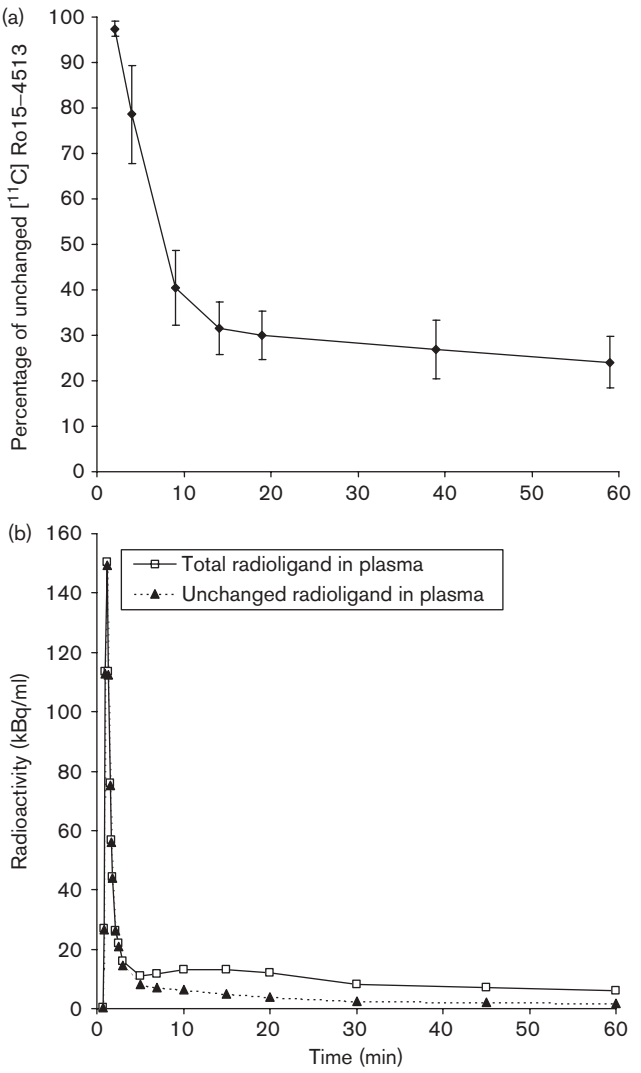

(a) Time course for the percentage of radioactivity in plasma corresponding to unchanged [^{11}C]Ro15-4513 in humans (mean ± SD; $n = 8$). (b) Time–activity curves for the concentration of total radioactivity in plasma (open square) and for the concentration of unchanged radioligand in plasma (triangle).

radioactivity for unchanged radioligand was used as an input function in two-compartment and three-compartment model analyses (Fig. 6).

The rate constants obtained from kinetic model approaches are shown in Table 1. The k_3/k_4 values obtained using three-compartment model analysis were high in the anterior cingulate cortex followed by insular cortex, hippocampus, amygdala, and, intermediate in the lateral temporal cortex, and low in the occipital cortex (Table 1).

Regarding the pons, the differences of AIC and SC were small between the two-compartment and three-compartment models, and the results of *F*-test did not show a significant improvement with the three-compartment model in four participants (Table 2). Regarding other regions except the pons, 39 ROIs of 48 (6 regions × 8 participants) showed significant improvement with three-compartment model, and similarly, three-compartment model showed lower AIC values in 41 ROIs and lower SC in 43 ROIs.

BP values obtained from simplified method analyses are shown in Table 3. The BP values obtained using graphical analysis without blood sampling ($BP_{graphical}$) correlated well with BP_{3CM} (Fig. 7a). The BP values obtained using SRTM analysis (BP_{SRTM})also correlated well with BP_{3CM} (Fig. 7b). In both relations, the correlation coefficient '*r*' was above 0.95, and the intercept was close to zero.

The reliability of estimated parameters was evaluated for graphical analysis without blood sampling and SRTM analysis by means of a computer simulation. In both methods, the variation of estimated BP increased as the noise increased (Fig. 8). The mean values of estimated BP deviated as the noise increased (Fig. 9). The mean BP and COV were 6.52 and 2.43%, respectively, for graphical analysis without blood sampling at 5% noise level, whereas these were 6.82 and 1.77% for SRTM analysis at the same noise level. At the 20% noise level, the mean BP and COV were 6.40 and 8.27% for graphical analysis without blood sampling, and these were 6.85 and 7.18% for SRTM analysis. COV for SRTM analysis were

Fig. 6

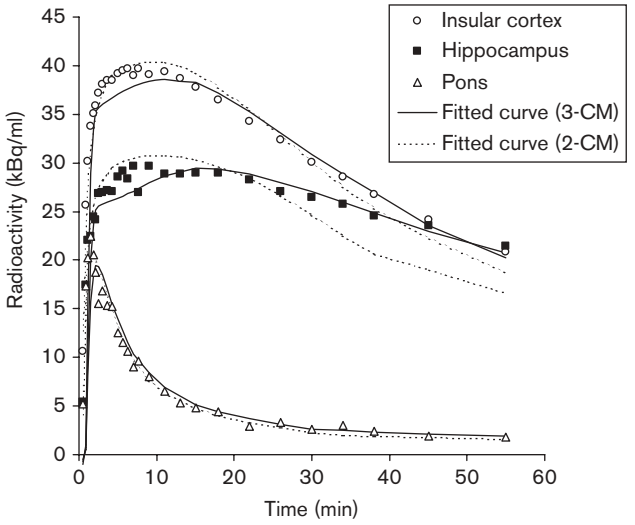

Measured tissue time–activity curves and corresponding fitted curves obtained by two-compartment (dashed lines) and three-compartment (solid lines) models in one participant.

smaller than those for graphical analysis without blood sampling in every noise level as shown in Fig. 8.

Discussion

The accumulation pattern of [^{11}C]Ro15-4513 in the human brain was consistent with previous reports [7,8,36]. As [^{11}C]Ro15-4513 has relatively high affinity for the α5 subunit-containing $GABA_A$/BZ receptor *in vitro* [15,16] and *in vivo* [17,36], the high uptake in the limbic areas would reflect the rich distribution of the α5 subunit-containing $GABA_A$/BZ receptor. Regional BPs in our study were in accordance with the regional DVs reported by Lingford-Hughes *et al.* [36] in terms of rank order. Distribution patterns of regional BPs in our study are concordant with the regional expression of α5 receptors *in vitro* in rats [44–46].

For the kinetic analysis, the time–activity curves of the pons were well described by both the two- and three-compartment models. BP of the pons obtained from three-compartment model was relatively small (0.18 ± 0.06).

Table 1 Rate constants obtained by 2-CM and 3-CM models

Region	K_1	k_2	K_1/k_2	k_3	k_4	k_3/k_4	$(K_1/k_2)(1+k_3/k_4)$
2-CM							
Hippocampus	0.22 ± 0.02	0.038 ± 0.005	5.89 ± 0.39				
Amygdala	0.22 ± 0.02	0.039 ± 0.004	5.63 ± 0.26				
Anterior cingulate cortex	0.31 ± 0.02	0.049 ± 0.006	6.39 ± 0.49				
Insular cortex	0.34 ± 0.03	0.057 ± 0.007	6.05 ± 0.37				
Lateral temporal cortex	0.29 ± 0.03	0.065 ± 0.009	4.55 ± 0.33				
Occipital cortex	0.32 ± 0.03	0.101 ± 0.013	3.22 ± 0.23				
Pons	0.27 ± 0.03	0.300 ± 0.034	0.89 ± 0.05				
3-CM							
Hippocampus	0.33 ± 0.03	0.40 ± 0.03	0.82 ± 0.03	0.57 ± 0.07	0.09 ± 0.02	6.49 ± 0.67	6.15 ± 0.43
Amygdala	0.31 ± 0.04	0.38 ± 0.05	0.82 ± 0.04	0.70 ± 0.05	0.12 ± 0.03	6.09 ± 0.48	5.81 ± 0.31
Anterior cingulate cortex	0.46 ± 0.04	0.57 ± 0.04	0.81 ± 0.03	0.90 ± 0.14	0.13 ± 0.02	7.02 ± 0.68	6.49 ± 0.50
Insular cortex	0.51 ± 0.06	0.63 ± 0.07	0.81 ± 0.03	0.90 ± 0.11	0.14 ± 0.02	6.66 ± 0.44	6.21 ± 0.40
Lateral temporal cortex	0.39 ± 0.05	0.48 ± 0.06	0.82 ± 0.04	0.91 ± 0.20	0.19 ± 0.04	4.73 ± 0.48	4.67 ± 0.34
Occipital cortex	0.41 ± 0.04	0.49 ± 0.04	0.82 ± 0.03	0.95 ± 0.21	0.32 ± 0.06	2.99 ± 0.37	3.31 ± 0.23
Pons	0.27 ± 0.03	0.33 ± 0.04	0.82 ± 0.04	0.02 ± 0.02	0.32 ± 0.55	0.18 ± 0.06	0.92 ± 0.04

2-CM, two-compartment model; 3-CM, three-compartment model.

Table 2 Comparison of 2-CM and 3-CM models for the description of [^{11}C]Ro15-4513 binding in the pons

Participant	Compartment model	K_1	k_2	k_3	k_4	k_3/k_4	RSS	AIC	SC	*F* statistics
A	2-CM	0.300	0.347	–	–	–	5.8	53	56	NS
	3-CM	0.298	0.363	0.020	0.275	0.072	5.6	56	55	
B	2-CM	0.224	0.240	–	–	–	9.1	66	69	$P<0.05$
	3-CM	0.242	0.298	0.024	0.116	0.208	5.9	57	57	
C	2-CM	0.260	0.274	–	–	–	4.6	47	50	NS
	3-CM	0.269	0.300	0.013	0.130	0.099	4.2	48	47	
D	2-CM	0.266	0.312	–	–	–	5.7	53	55	$P<0.05$
	3-CM	0.275	0.347	0.008	0.051	0.151	3.9	46	45	
E	2 CM	0.296	0.335	–	–	–	16.1	82	84	$P<0.05$
	3-CM	0.307	0.379	0.018	0.142	0.128	11.5	76	75	
F	2-CM	0.255	0.293	–	–	–	12.9	76	78	NS
	3-CM	0.243	0.291	0.052	1.669	0.031	17.0	87	86	
G	2-CM	0.250	0.316	–	–	–	30.1	99	102	NS
	3-CM	0.238	0.303	0.002	0.010	0.171	33.3	106	105	
H	2-CM	0.264	0.299	–	–	–	15.3	80	83	$P<0.05$
	3-CM	0.278	0.355	0.032	0.198	0.162	9.5	71	70	

2-CM, two-compartment model; 3-CM, three-compartment model; AIC, Akaike information criterion; NS, not significant; RSS, residual square sum; SC, Schwarz criterion.

Table 3 Comparison of BP values obtained using three quantitative approaches

	Kinetic analysis Three-compartment model	Linear graphical analysis	Simplified reference tissue model analysis
Region	$BP_{3\text{-}CM}$	BP_{Logan}	BP_{SRTM}
Pons	0.13 ± 0.06	NA	NA
Hippocampus	6.49 ± 0.67	5.85 ± 0.63	5.98 ± 0.65
Amygdala	6.09 ± 0.48	5.42 ± 0.51	5.55 ± 0.57
Anterior cingulate	7.02 ± 0.68	6.22 ± 0.68	6.30 ± 0.73
Insular cortex	6.66 ± 0.44	5.96 ± 0.58	5.99 ± 0.59
Lateral temporal cortex	4.73 ± 0.48	4.25 ± 0.58	4.25 ± 0.59
Occipital cortex	2.99 ± 0.37	2.73 ± 0.34	2.71 ± 0.34

Values are mean ± SD (n = 8).
BP, binding potential; NA, not applicable; SRTM, simplified reference tissue model.

The difference of AIC and SC from the two-compartment to three-compartment model and the result of the F-test supported the use of the two-compartment model for the pons. These results were consistent with previous studies, indicating negligible density of the BZ receptors in the pons [5,11,17]. The time–activity curves for most ROIs with specific binding were well described by the three-compartment model compared with the two-compartment model. This would indicate that the specific binding sites exist in these regions.

There were high correlations between $BP_{graphical}$ and BP_{3CM} and between BP_{SRTM} and BP_{3CM}, and the intercept of regression line was near zero (Fig. 7a and b), although BPs estimated with graphical and SRTM analyses without blood sampling were smaller than those with NLSF analysis (Table 3). This would indicate that [^{11}C]Ro15-4513 binding could be practically evaluated without blood sampling by using the pons as the reference region. Although k_3 and k_4 can be estimated individually by the NLSF analysis with three-compartment model, these parameter estimates are sensitive to the noise in general. As graphical and SRTM analyses were more simple and robust than NLSF method with three-compartment model, the simplified method would be more practical in clinical research with [^{11}C]Ro15-4513.

In the simulation study, the deviation of BPs obtained from both graphical analysis and SRTM became larger as the noise increased. In the simulation study, the bias and variation of estimated values for SRTM analysis were smaller than those for graphical analysis in every noise level, especially in high noise level. In the graphical method, BPs were affected by the tendency of underestimation in DVR. Furthermore, in the graphical method, DV was estimated as a slope of points after equilibration time, and the reliability of estimated BP varies by data points used for estimation. BPs obtained from SRTM analysis seemed more reliable than those from graphical analysis.

Fig. 7

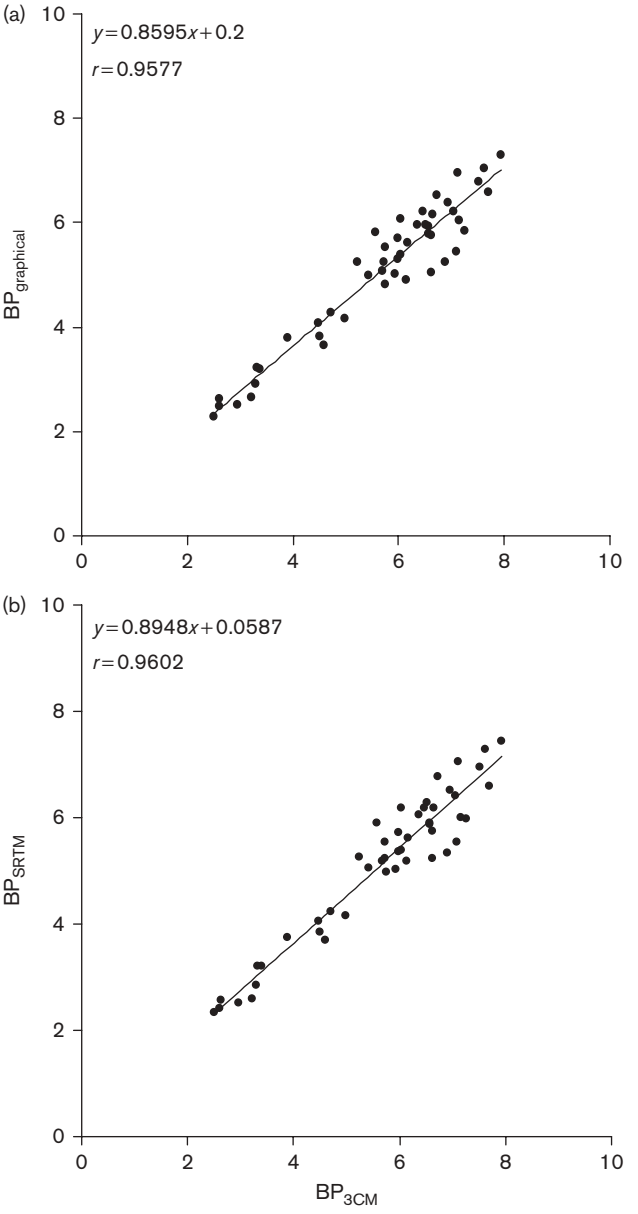

(a) Correlation between binding potential (BP) values obtained using graphical analysis without blood sampling ($BP_{graphical}$) and BP values obtained using the three-compartment model analysis (BP_{3CM}).
(b) Correlation between BP values obtained using simplified reference tissue model (SRTM) analysis (BP_{SRTM}) and BP values obtained using the three-compartment model analysis (BP_{3CM}).

The functions of α5 subunit of $GABA_A$/BZ receptor have been focused recently in relation to the memory and pathophysiology of neuropsychiatric disorders. As α5 subunit knockout mice showed enhanced performance in learning and memory task, the amnesic action of BZ may be related to α5 subunit-containing $GABA_A$/BZ receptor in the hippocampus [47]. Increased mRNA of α5 subunit-containing $GABA_A$/BZ receptor in the prefrontal

Fig. 8

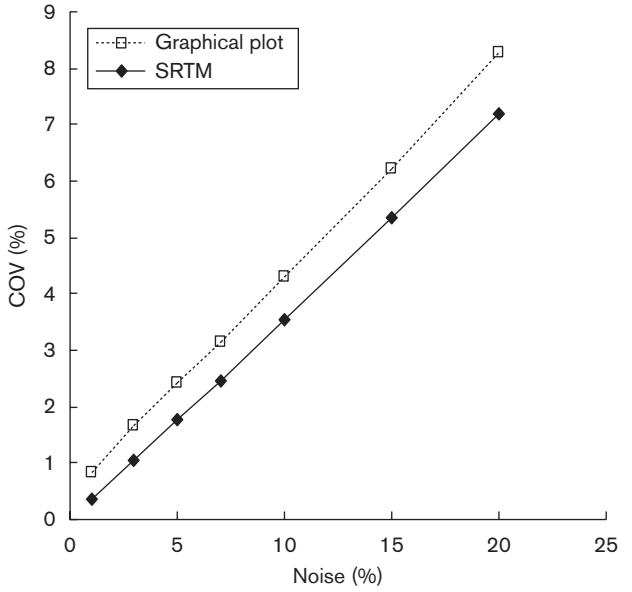

Relationship between noise and coefficient of variance (COV) of estimated binding potentials for graphical analysis without blood sampling (open square) and simplified reference tissue model (SRTM) analysis (closed circle).

Fig. 9

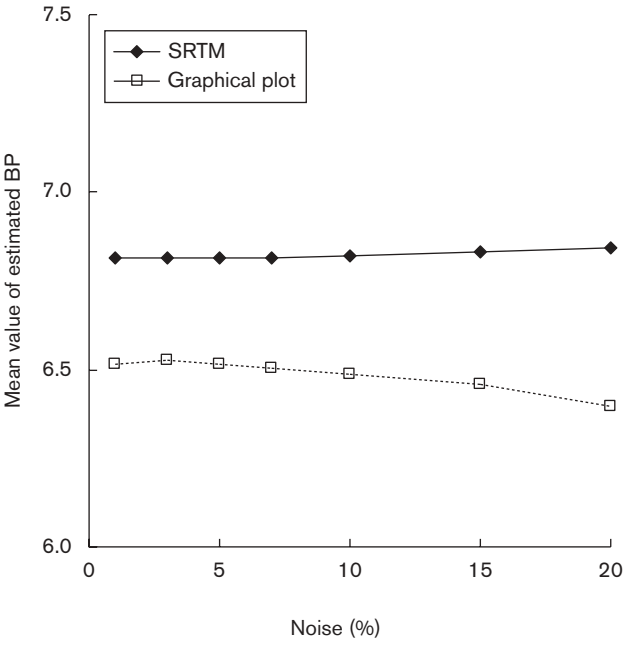

Relationship between noise and mean binding potentials for graphical analysis without blood sampling (graphical) (open square) and simplified reference tissue model analysis (closed circle).

cortex has been reported in postmortem study of schizophrenia patients [30]. The association between the genotype of α5 subunit and bipolar affective disorder and was reported [31]. α5 subunit-containing $GABA_A$/BZ receptors were reported to be preserved in the hippocampus of Alzheimer's disease [29]. [^{11}C]Ro15-4513 can be a useful tool for in-vivo investigation of α5 subunit-containing $GABA_A$/BZ receptors in the human brain.

There are some limitations of this study. Pretreatment studies were not performed in this study. It was not shown that the accumulation of [^{11}C]Ro15-4513 represents only the specific binding to $GABA_A$/BZ receptors α5 subunit. Ro15-4513 has 10–20-fold higher affinity for α5 subunit-containing $GABA_A$/BZ receptor ($K_i = 0.7$ nmol/l) compared with α1, α2, and α3 subunits ($K_i = 7$–10 nmol/l) *in vitro* [48]. The monkey pretreatment study showed that zolpidem with affinity for α1, α2, α3 subunits of $GABA_A$/BZ receptor fully inhibited [^{11}C]Ro15-4513 binding in the occipital cortex and cerebellum, whereas only about 23% of [^{11}C]Ro15-4513 binding were blocked in the anterior cingulate cortex [17]. It would indicate that high accumulation of [^{11}C]Ro15-4513 in the frontotemporal limbic regions mainly represent the binding to $GABA_A$/BZ receptor α5 subunit. However, [^{11}C]Ro15-4513 binding in the occipital cortex and cerebellum would not reflect the binding to α5 subunit-containing $GABA_A$/BZ receptor. When the regional change of [^{11}C]Ro15-4513 binding is interpreted in future clinical study, the affinity characters should be taken into consideration.

Conclusion

The regional distribution and binding kinetics of [^{11}C]Ro15-4513 were examined in the living human brain. The time–activity curves were well described by the three-compartment model using metabolite-corrected plasma input function, and the specific binding in the pons was small enough to use as a reference region. BPs estimated by both graphical analysis and SRTM analysis using the pons as the reference region were highly correlated with those by three-compartment model. In the simulation study, the BPs obtained from SRTM analysis seemed to be more reliable than graphical analysis.

Acknowledgements

This study was supported by CREST, Japan Science and Technology Corporation (JST), Saitama, Japan, and the PET project of National Institute of Radiological Sciences. This study was also supported in part by a Grant-in Aid for Molecular Imaging Program from the Ministry of Education, Culture, Sports, Science and Technology (MEXT), Japanese Government.

References

1 Sigel E, Buhr A. The benzodiazepine binding site of $GABA_A$ receptors. *Trends Pharmacol Sci* 1997; **18**:425–429.
2 Mehta AK, Ticku MK. An update on $GABA_A$ receptors. *Brain Res Brain Res Rev* 1999; **29**:196–217.

3 Shinotoh H, Yamasaki T, Inoue O, Itoh T, Suzuki K, Hashimoto K, *et al*. Visualization of specific binding sites of benzodiazepine in human brain. *J Nucl Med* 1986; **27**:1593–1599.
4 Pappata S, Samson Y, Chavoix C, Prenant C, Maziere M, Baron JC. Regional specific binding of [^{11}C]Ro15 1788 to central type benzodiazepine receptors in human brain: quantitative evaluation by PET. *J Cereb Blood Flow Metab* 1988; **8**:304–313.
5 Abadie P, Baron JC, Bisserbe JC, Boulenger JP, Rioux P, Travere JM, *et al*. Central benzodiazepine receptors in human brain: estimation of regional Bmax and KD values with positron emission tomography. *Eur J Pharmacol* 1992; **213**:107–115.
6 Halldin C, Farde L, Litton JE, Hall H, Sedvall G. [^{11}C]Ro 15-4513, a ligand for visualization of benzodiazepine receptor binding. *Psychopharmacology* 1992; **108**:16–22.
7 Inoue O, Suhara T, Itoh T, Kobayashi K, Suzuki K, Tateno Y. In vivo binding of [^{11}C]Ro15-4513 in human brain measured with PET. *Neurosci Lett* 1992; **145**:133–136.
8 Suhara T, Inoue O, Kobayashi K, Suzuki K, Itoh T, Tateno Y. No age-related changes in human benzodiazepine receptor binding measured by PET with [^{11}C]Ro 15-4513. *Neurosci Lett* 1993; **159**:207–210.
9 Foged C, Halldin C, Loc'h C, Maziere B, Pauli S, Maziere M, *et al*. Bromine-76 and carbon-11 labelled NNC 13-8199, metabolically stable benzodiazepine receptor agonists as radioligands for positron emission tomography. *Eur J Nucl Med* 1997; **24**:1261–1267.
10 Millet P, Graf C, Buck A, Walder B, Westera G, Broggini C, *et al*. Similarity and robustness of PET and SPECT binding parameters for benzodiazepine receptors. *J Cereb Blood Flow Metab* 2000; **20**:1587–1603.
11 Onoe H, Tsukada H, Nishiyama S, Nakanishi S, Inoue O, Langstrom B, *et al*. A subclass of $GABA_A$/benzodiazepine receptor exclusively localized in the limbic system. *Neuroreport* 1996; **8**:117–122.
12 Nakano T, Satoh T, Mori K, Inoue O. Imaging of the super high affinity binding sites for [^{3}H]Ro15-4513 in rat hippocampus: comparison between in vitro and in vivo binding. *Neurosci Lett* 1998; **250**:161–164.
13 Lüddens H, Korpi ER, Seeburg PH. $GABA_A$/benzodiazepine receptor heterogeneity: neurological implications. *Neuropharmacology* 1995; **34**:245–254.
14 Barnard EA, Skolnick P, Olsen RW, Mohler H, Sieghart W, Biggio G, *et al*. Subtypes of gamma-aminobutyric acid A receptors: classification on the basis of subunit structure and receptor function. *Pharmacol Rev* 1998; **50**:291–313.
15 Lüddens H, Seeburg PH, Korpi ER. Impact of beta and gamma variants on ligand-binding properties of gamma-aminobutyric acid type A receptors. *Mol Pharmacol* 1994; **45**:810–814.
16 Wieland HA, Lüddens H. Four amino acid exchanges convert a diazepam-insensitive, inverse agonist-preferring $GABA_A$ receptor into a diazepam-preferring $GABA_A$ receptor. *J Med Chem* 1994; **37**:4576–4580.
17 Maeda J, Suhara T, Kawabe K, Okauchi T, Obayashi S, Hojo J, *et al*. Visualization of α5 subunit of GABAA/benzodiazepine receptor by [^{11}C]Ro15-4513 using positron emission tomography. *Synapse* 2003; **47**:200–208.
18 Rudolph U, Crestani F, Benke D, Brunig I, Benson JA, Fritschy JM, *et al*. Benzodiazepine actions mediated by specific gamma-aminobutyric $acid_A$ receptor subtypes. *Nature* 1999; **401**:796–800.
19 Low K, Crestani F, Keist R, Benke D, Brunig I, Benson JA, *et al*. Molecular and neuronal substrate for the selective a attenuation of anxiety. *Science* 2000; **290**:131–134.
20 Tobler I, Kopp C, Deboer T, Rudolph U. Diazepam-induced changes in sleep: role of the alpha 1 $GABA_A$ receptor subtype. *Proc Natl Acad Sci U S A* 2001; **98**:6464–6469.
21 Smith TA. Type A gamma-aminobutyric acid ($GABA_A$) receptor subunits and benzodiazepine binding: significance to clinical syndromes and their treatment. *Br J Biomed Sci* 2001; **58**:111–121.
22 Smith AJ, Alder L, Silk J, Adkins C, Fletcher AE, Scales T, *et al*. Effect of alpha subunit on allosteric modulation of ion channel function in stably expressed human recombinant gamma-aminobutyric $acid_A$ receptors determined using ^{36}Cl ion flux. *Mol Pharmacol* 2001; **59**:1108–1118.
23 Casula MA, Bromidge FA, Pillai GV, Wingrove PB, Martin K, Maubach K, *et al*. Identification of amino acid residues responsible for the alpha5 subunit binding selectivity of L-655,708, a benzodiazepine binding site ligand at the $GABA_A$ receptor. *J Neurochem* 2001; **77**:445–451.
24 Navarro JF, Buron E, Martin-Lopez M. Anxiogenic-like activity of L-655,708, a selective ligand for the benzodiazepine site of $GABA_A$ receptors which contain the alpha-5 subunit, in the elevated plus-maze test. *Prog Neuropsychopharmacol Biol Psychiatr* 2002; **26**:1389–1392.
25 Kralic JE, O'Buckley TK, Khisti RT, Hodge CW, Homanics GE, Morrow AL. GABAA receptor alpha-1 subunit deletion alters receptor subtype assembly, pharmacological and behavioral responses to benzodiazepines and zolpidem. *Neuropharmacology* 2002; **43**:685–694.
26 Crestani F, Low K, Keist R, Mandelli M, Mohler H, Rudolph U. Molecular targets for the myorelaxant action of diazepam. *Mol Pharmacol* 2001; **59**:442–445.
27 Mohler H, Crestani F, Rudolph U. $GABA_A$-receptor subtypes: a new pharmacology. *Curr Opin Pharmacol* 2001; **1**:22–25.
28 Lewohl JM, Huygens F, Crane DI, Dodd PR. $GABA_A$ receptor alpha-subunit proteins in human chronic alcoholics. *J Neurochem* 2001; **78**:424–434.
29 Howell O, Atack JR, Dewar D, Mckernan RM, Sur C. Density and pharmacology of α5 subunit-containing $GABA_A$ receptors are preserved in hippocampus of Alzheimer's disease patients. *Neuroscience* 2000; **98**:669–675.
30 Impagnatiello F, Guidotti AR, Pesold C, Dwivedi Y, Caruncho H, Pisu MG, *et al*. A decrease of reelin expression as a putative vulnerability factor in schizophrenia. *Neurobiology* 1998; **95**:15718–15723.
31 Papadimitriou GN, Dikeos DG, Karadima G, Avramopoulos D, Daskalopoulou EG, Vassilopoulos D, *et al*. Association between the $GABA_A$ receptor α5 subunit gene locus ($GABRA_5$) and bipolar affective disorder. *Am J Med Genetics.* 1998; **81**:73–80.
32 Ohnuma T, Augood SJ, Arai H, Mckenna PJ, Emson PC. Measurement of GABAergic parameters in the prefrontal cortex in schizophrenia: focus on GABA content, $GABA_A$ receptor α-1 subunit messenger RNA and human GABA transporter-1 (HGAT-1) messenger RNA expression. *Neuroscience* 1999; **93**:441–448.
33 Akbarian S, Huntsman MM, Kim JJ, Tafazzoli A, Potkin SG, Bunney WE Jr, *et al*. $GABA_A$ receptor subunit gene expression in human prefrontal cortex: comparison of schizophrenics and controls. *Cerebral Cortex* 1995; **5**:550–560.
34 Byerley W, Bailey MES, Hicks AA, Riley BP, Darlison MG, Holik J, *et al*. Schizophrenia and $GABA_A$ receptor subunit genes. *Psychiatr Genetics* 1995; **5**:23–29.
35 Guidotti A, Auta J, Davis JM, Dong E, Grayson DR, Veldic M, *et al*. GABAergic dysfunction in schizophrenia: new treatment strategies on the horizon. *Psychopharmacology (Berlin)* 2005; **180**:191–205.
36 Lingford-Hughes A, Hume SP, Feeney A, Hirani E, Osman S, Cunnungham VJ, *et al*. Imaging the GABA-benzodiazepine receptor subtype containing the α5-subunit in vivo with [^{11}C]Ro15 4513 positron emission tomography. *J Cereb Blood Flow Metab* 2002; **22**:878–889.
37 Mintun MA, Raichle ME, Kilbourn MR, Wooten GF, Welch MJ. A quantitative model for the in vivo assessment of drug binding sites with positron emission tomography. *Ann Neurol* 1984; **15**:217–227.
38 Marquest DW. An algorithm for least-squares estimation on non-linear parameters. *J Soc Ind Appl Math* 1963; **11**:431–441.
39 Akaike H. A new look at statistical model identification. *IEEE Trans Automat Contr* 1974; **19**:716–723.
40 Schwarz G. Estimating the dimension of a model. *Ann Stat* 1978; **6**:461–464.
41 Logan J, Fowler JS, Volkow ND, Wang GJ, Ding YS, Alexoff DL. Distribution volume ratios without blood sampling from graphical analysis of PET data. *J Cereb Blood Flow Metab* 1996; **16**:834–840.
42 Lammertsma AA, Hume SP. Simplified reference tissue model for PET receptor studies. *Neuroimage* 1996; **4**:153–158.
43 Ikoma Y, Toyama H, Yamada T, Uemura K, Kimura Y, Senda M, *et al*. Creation of a dynamic digital phantom and its application to a kinetic analysis. *Jpn J Nucl Med* 1998; **35**:293–303.
44 Fritschy JM, Mohler H. GABAA-receptor heterogeneity in the adult rat brain: differential regional and cellular distribution of seven major subunit. *J Comp Neurol* 1995;**359**:154–194.
45 Sur C, Fresu L, Howell O, McKernan RM, Atack JR. Autoradiographic localization of alpha5 subunit-containing GABAA receptors in rat brain. *Brain Res* 1999;**822**:265–270.
46 Pirker S, Schwarzer C, Wieselthaler A, Sieghart W, Sperk G. GABAA receptors: immunocytochemical distribution of 13 subunits in the adult rat brain. *Neuroscience* 2000; **101**:815–880.
47 Collinson N, Kuenzi FM, Jarolimek W, Maubch KA, Cothliff R, Sur C, *et al*. Enhanced learning and memory and altered GABAergic synaptic transmission in mice lacking the alpha 5 subunit of the $GABA_A$ receptor. *J Neurosci* 2002; **22**:5572–5580.
48 Hadingham KL, Wingrove P, Le Bourdelles B, Palmer KJ, Ragan CI, Whiting PJ. Cloning of cDNA sequences encoding human alpha 2 and alpha 3 gamma-aminobutyric acidA receptor subunits and characterization of the benzodiazepine pharmacology of recombinant alpha 1-, alpha 2-, alpha 3-, and alpha 5-containing human gamma-aminobutyric acidA receptors. *Mol Pharmacol* 1993; **43**:970–975.